Macromolecules

pubs.acs.org/Macromolecules Article

Structure of Polyelectrolyte Brushes on Polarizable Substrates

Jiaxing Yuan, Hanne S. Antila, and Erik Luijten*

Cite This: *Macromolecules* 2020, 53, 2983−2990 Read Online

ACCESS | Metrics & More | Article Recommendations

ABSTRACT: Understanding the structural response of polyelectrolyte brushes to variation in both intrinsic and external properties is highly relevant for their application as functionalized interfaces and components of nanodevices. Using coarse-grained simulations, we examine an aspect that is largely unexplored, namely the dielectric mismatch between the solvent and the substrate. We systematically study how this permittivity contrast alters the brush structure over a range of Bjerrum length, polymer charge density, counterion size and valency, salt concentration, polymer grafting density, and external electric field. In addition to the expected brush contraction near metallic substrates and expansion on low-permittivity substrates, we find various regimes where variation of the substrate properties qualitatively alters the brush response.

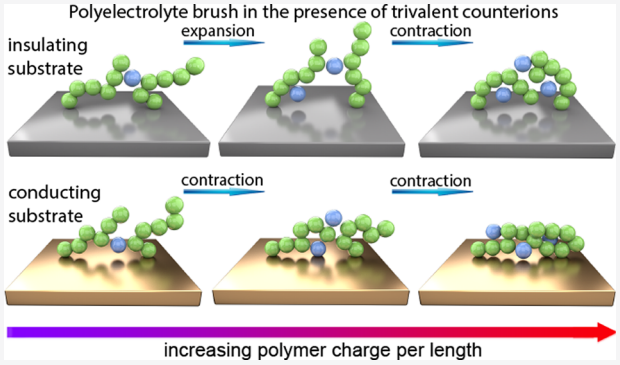

1. INTRODUCTION

Polyelectrolyte brushes (PEBs), assemblies of charged polymers (polyelectrolytes, PEs) grafted onto a solid substrate, are encountered in a wide range of applications, including the design of functionalized interfaces and of nanochannels with controllable properties.[1,2] In the latter, one exploits the reversible collapse−extension transition of PEBs that occurs in response to variation in temperature,[3,4] electric field,[5−7] pH,[8,9] or photoirradiation frequency[10] to open or block a nanochannel and thereby control the transport of solvent and solutes. The modulation of interfacial wetting properties through structural changes in the PEB that result from changes in salt concentration[11] or pH[12] and that either permit water penetration into the PEB or exclude water from it provides a practical example of surface functionalization by PEBs. They can also be used to control the interactions between colloidal building blocks. For example, pH-switchable aggregation and disaggregation of Janus colloids has been achieved by coating the hemispheres with distinct types of PEBs.[13]

Given their prevalence, understanding the structure of PEBs under different conditions has been the subject of considerable theoretical, computational, and experimental research efforts. Particle-based simulations have been performed to investigate the dependence of brush behavior on salt concentration,[14−20] solvent quality,[18,21−23] and permittivity,[21,24,25] temperature,[23] external electric field,[5,6,26−28] grafting density,[6,17,19,20,24,29,30] polymer charge density,[20,24−26,31] chain stiffness,[16,27] and counterion valency,[19,31−35] along with comparisons to scaling predictions,[14,22,29,36−38] self-consistent field theories,[17,39−43] and density-functional theories.[44] Experimental techniques, such as dynamic light scattering,[45] atomic force microscopy,[35] and dielectric spectroscopy,[46] have been utilized to directly visualize the PEB structures and to quantify their structure (e.g., brush thickness) at different conditions.

Our interest here lies in the effect of substrate properties on PEB structure. Prior simulations have investigated the impact of surface charges[24,25,47] on interfacial brush and ion behavior, but the role of the dielectric properties of the substrate has been ignored, apart from one computational study of a spherical PEB constructed on a silica nanoparticle.[48] We note that substrates in practical applications range from metallic[4,49] to insulating.[50,51] Moreover, we speculate that surface effects are particularly important in brushes consisting of short chains, which are becoming increasingly relevant as advances in manufacturing techniques continue to push the sizes of PEB-functionalized nanochannels down to a few nanometers.[52] Short polyelectrolytes have also been grafted to outer surfaces, for example, to create oligonucleotide-functionalized gold nanoparticles for the detection of complementary DNA fragments.[53]

We employ coarse-grained molecular dynamics (MD) simulations to study the effect of substrate permittivity on the structure of a PEB consisting of short chains and on the behavior of counterions within these assemblies. We systematically map out how dielectric effects change the brush

Received: December 30, 2019
Revised: March 21, 2020
Published: April 6, 2020

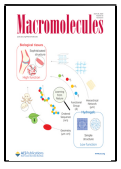

https://dx.doi.org/10.1021/acs.macromol.9b02749
Macromolecules 2020, 53, 2983−2990

response to variation in Bjerrum length (i.e., solvent permittivity or temperature), polymer charge, counterion valency and size, salt concentration, grafting density, and electric field. This report is organized as follows. We start with an overview of the simulation model and computational details in section 2. In section 3, we explore the structural variation of a PEB on three types of substrates (insulating, conducting, and nonpolarizable interfaces). We first vary the Bjerrum length (section 3.1) and polymer charge density (section 3.2) and then proceed to examine the role of counterion valency (section 3.3) and size (section 3.4) along with salt concentration, grafting density (section 3.5), and electric field (section 3.6). Section 4 provides a brief summary.

2. MODEL AND METHOD

We employ the same coarse-grained model as in our recent work on ion transport through PEBs.[54] We model anionic PE oligomers as bead−spring chains[55,56] of $N = 10$ monomers, each carrying an elementary charge $-e$. The simulated system consists of 6×6 linear chains uniformly grafted onto a planar substrate (located at $z = 0$) in a square lattice pattern with spacing $d = \Gamma^{-1/2}$, where Γ is the grafting density, i.e., the number of chains per unit area. We primarily focus on a salt-free and sparse PEB at low grafting density $\Gamma = 0.02\sigma^{-2}$ with monovalent counterions (charge e) of the same size as the monomers. However, later on we also vary salt concentration, grafting density, counterion valency, and ion size to examine their effect on PEB structure and responsiveness to substrate permittivity.

The brush monomers and counterions are represented as spheres of identical mass m and diameters σ_b and σ_c, respectively. The excluded-volume interaction between ions and monomers is modeled by a shifted-truncated Lennard-Jones (LJ) potential

$$U_{LJ}(r_{ij}) = \begin{cases} 4\varepsilon_{LJ}\left[\left(\frac{\bar{\sigma}_{ij}}{r_{ij}}\right)^{12} - \left(\frac{\bar{\sigma}_{ij}}{r_{ij}}\right)^{6} + \frac{1}{4}\right] & r_{ij} \le r_{cut} \\ 0 & r_{ij} > r_{cut} \end{cases} \quad (1)$$

where r_{ij} is the center-to-center distance between particles i and j, $\bar{\sigma}_{ij} = (\sigma_i + \sigma_j)/2$ is their average diameter (center-to-center distance at contact), and $r_{cut} = 2^{1/6}\bar{\sigma}_{ij}$ denotes the cutoff distance. The diameter of the monomers is our unit of length $\sigma = \sigma_b$, and the unit of energy is $\varepsilon_{LJ} = k_BT/1.2$, where k_B is Boltzmann's constant and T the absolute temperature. Neighboring monomers along a chain are bonded through a harmonic potential

$$U_{bond}(r_{ij}) = \frac{1}{2}K(r_{ij} - R_0)^2 \quad (2)$$

with spring constant $K = 400\varepsilon_{LJ}/\sigma^2$ and bond length $R_0 = 2^{1/6}\sigma$. The electrostatic interaction between a pair of particles of valencies q_i and q_j is given by

$$U_{Coul}(r_{ij}) = k_BTl_B\frac{q_iq_j}{r_{ij}} \quad (3)$$

where $l_B = e^2/(4\pi\kappa_{sol}k_BT)$ (κ_{sol} defined below) is the Bjerrum length. These interactions are taken into account via the particle−particle particle−mesh (PPPM) algorithm[57] with a relative accuracy of 10^{-5}.

The simulation cell is 2D-periodic in the x- and y-directions with dimensions $[0, L] \times [0, L] \times [0, L_z]$, where L will be tuned to vary the grafting density and $L_z = 12.5\sigma$. The ions and monomers are confined between purely repulsive LJ walls ($\varepsilon_{wall} = \varepsilon_{LJ}$; $\sigma_{wall} = 0.5\sigma_i$) at $z = 0$ and $z = L_z$ and are immersed in a continuum medium of dielectric permittivity κ_{sol} representing the solvent. There is no dielectric mismatch between the medium and the upper wall, but the substrate has a permittivity κ_{sub}. A schematic of the simulated system is presented in Figure 1.

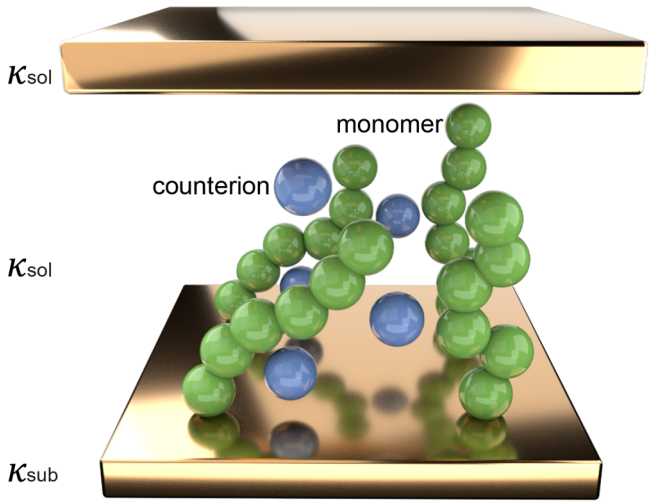

Figure 1. Schematic of the simulated system. Polyelectrolytes (green) are described as bead−spring chains and immersed in implicit solvent with permittivity κ_{sol} along with the counterions (blue). The chains are grafted in a square pattern onto a substrate that has dielectric permittivity κ_{sub}.

The dielectric mismatch between the solvent and the substrate gives rise to surface polarization charge, which can be represented using image charges.[58,59] The self-image interaction between a particle of valency q_i and its own image charge is

$$U^{self}_{Coul}(z_i) = k_BTl_Bq_i^2\frac{\Delta}{4z_i} \quad (4)$$

where $\Delta = (\kappa_{sol} - \kappa_{sub})/(\kappa_{sol} + \kappa_{sub})$ is the dielectric mismatch between the solvent and the substrate. A conducting substrate (attractive surface polarization) corresponds to $\Delta = -1$ and an insulating substrate (repulsive polarization) to $\Delta > 0$ (we consider the limiting value $\Delta = 1$). A nonpolarizable substrate has $\kappa_{sol} = \kappa_{sub}$, so that $\Delta = 0$. Including dielectric effects, the total pairwise electrostatic interaction between two particles of valency q_i and q_j is therefore

$$U^{ij}_{Coul}(r_{ij}) = k_BTl_Bq_iq_j\left(\frac{1}{r_{ij}} + \frac{\Delta}{\sqrt{r_{ij}^2 + 4z_iz_j}}\right) \quad (5)$$

We have modified the PPPM algorithm to incorporate eqs 4 and 5. The actual simulation cell spans from $z = -L_z$ to $z = L_z$ to accommodate image charges, and the (quasi-2D) slab geometry is expanded to a 3D-periodic system by means of a 50σ thick vacuum layer, accompanied by a slab correction[60] to eliminate artifacts arising from the periodicity in the z dimension.

https://dx.doi.org/10.1021/acs.macromol.9b02749
Macromolecules 2020, 53, 2983−2990

We employ the *NVT* ensemble in which the temperature is controlled by a Langevin thermostat with damping time τ, where $\tau = (m\sigma^2/\varepsilon_{LJ})^{1/2}$ is the LJ unit of time. The positions and velocities are updated by using the velocity-Verlet algorithm with a time step of 0.01τ. We start from a fully stretched configuration and equilibrate the polymer chains for $10^4\tau$. The subsequent production runs last for $10^5\tau$, during which the configuration is sampled every 10τ. To quantify the system structure, we define the average brush height as $H_B = \left(\int_0^{L_z} \rho_B(z) z\, dz\right) / \left(\int_0^{L_z} \rho_B(z)\, dz\right)$ and the average counterion height as $H_c = \left(\int_0^{L_z} \rho_c(z) z\, dz\right) / \left(\int_0^{L_z} \rho_c(z)\, dz\right)$, where $\rho_b(z)$ and $\rho_c(z)$ are the number density distributions of the monomers and counterions, respectively.

3. RESULTS AND DISCUSSION

3.1. Effect of Temperature and Solvent Permittivity.

The dimensionless Manning parameter $\xi = l_B\lambda$, where $-e\lambda$ is the polymer charge per unit length, provides a useful way of quantifying the electrostatic coupling between ions and polyelectrolytes.[61] For polyelectrolytes in solution, Manning theory predicts a counterion condensation transition, controlled by the balance between counterion release entropy and electrostatic binding energy, at $\xi = 1/q$, with q the counterion valency. This condensation transition occurs in PEBs as well and affects the brush structure.[25] There are two independent ways of altering ξ, namely, either variation of the Bjerrum length l_B (by varying temperature or solvent permittivity), which we examine in the present section, or variation of the polymer charge density, which we pursue in section 3.2. The Bjerrum length controls the strength of *all* electrostatic interactions, whereas variation of λ alters all interactions involving monomer charges, including interactions between free charges and the monomer-induced substrate polarization charge, but not (directly) the interactions between ions and between ions and their image charges.

Figure 2a presents the brush height H_b and counterion height H_c of a sparse ($\Gamma = 0.02\sigma^{-2}$) and salt-free PEB as a function of l_B. We observe a nonmonotonic variation of PEB height, in line with previous simulations:[21,24,25,62] decreasing solvent permittivity (or temperature)—i.e., increasing Bjerrum length l_B—causes an initial expansion because of enhancement of intra- and interpolymer repulsion, followed by a contraction at $\xi^* \approx 1$ as the onset of ion condensation onto the chains starts to reduce the counterion osmotic pressure and the repulsive polymer−polymer interactions. At high Bjerrum lengths, this collapse may be further enhanced by the formation of localized monomer−ion pairs, resulting in attractive dipolar intrapolymer interactions, as was observed for free polyelectrolytes.[62] Accordingly, H_c monotonically decreases as ions are absorbed into the brush by the enhanced polymer−ion interactions.

Interestingly, the coupling strength ξ^* at which we observe a maximum in the brush height, followed by a contraction because of the onset of counterion condensation, aligns very well with the prediction of Manning theory. Various aspects of our system differ from the assumptions in this theory, including the flexibility and short length of the chains, finite ion size, and the interaction between neighboring chains. The last effect is likely weak due to the sparse brush density. In dense brushes ξ^* shifts,[25] as the chains no longer behave similar to free polyelectrolytes and interpolymer interactions contribute to the overall brush height. In the following sections, we will demonstrate how other factors affect the onset of ion condensation into the brush. This underlines that the applicability of Manning theory to the system studied here is merely qualitative.

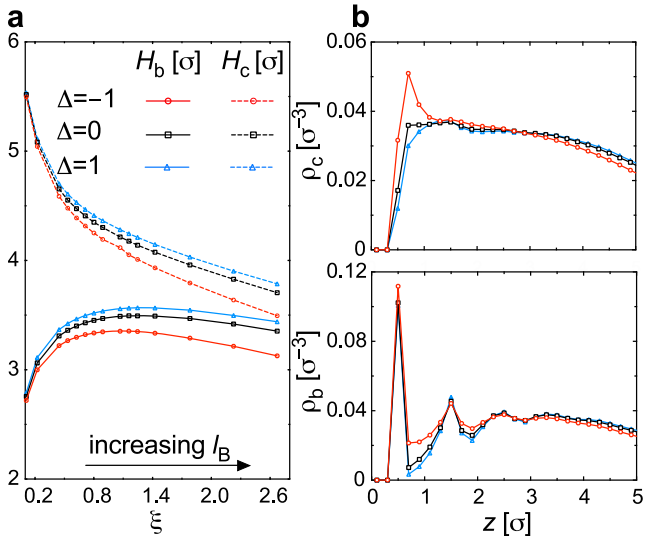

Figure 2. Effect of Bjerrum length on brush height and counterion distribution for different substrate permittivities. (a) Brush height H_b (solid lines) and counterion height H_c (dashed lines) as a function of Manning parameter ξ (increasing l_B). Different colors correspond to nonpolarizable ($\Delta = 0$, black), metallic ($\Delta = -1$, red), and insulating ($\Delta = 1$, blue) substrates. (b) Density distributions of counterions ρ_c (top) and monomers ρ_b (bottom) as a function of the distance z to the substrate for Bjerrum length $l_B = 3\sigma$ and polymer charge per length $-e\lambda = -0.89e/\sigma$.

Figure 2a also illustrates the effect of substrate permittivity on brush structure. A conducting substrate reduces the brush height, whereas a PEB grafted onto an insulating interface is expanded. This effect is less obvious than it may seem due to the interaction between counterions and the polarization charge induced by monomers, and vice versa. The dielectric modulation of brush behavior is best understood from the distributions of the different charged components in the system. We illustrate this for the parameter choice $l_B = 3\sigma$ and $-e\lambda = -e/(2^{1/6}\sigma) \approx -0.89e/\sigma$, the rightmost points in Figure 2a. Both the counterion distributions (Figure 2b, top) and the monomer distributions (Figure 2b, bottom) are affected by the surface polarization, with the strongest effects in the interfacial region. Repulsive polarization ($\Delta = 1$) has only a weak effect because of the inability of grafted monomers to be fully repelled from the surface, which then propagates to the counterion distribution via electrostatic ion−monomer binding. The monomer depletion seen here bears resemblance to the observation of reduced adsorption of free polyelectrolytes onto a low-permittivity substrate.[63] In contrast, attractive polarization significantly enhances the monomer and ion concentrations near the brush substrate.

The dielectric effects are strongest at large l_B (small solvent permittivity or low temperature) due to the stronger electrostatic coupling between the surface polarization and both the ions and the monomers. This, along with the ability of ion−polarization interactions to alter the onset of ion condensation, causes a shift in the coupling strength ξ^* at which the brush height reaches a maximum. PEBs on a

https://dx.doi.org/10.1021/acs.macromol.9b02749
Macromolecules 2020, 53, 2983−2990

conducting substrate reach their most expanded state at a smaller coupling than those grafted on an insulating interface.

The surface polarization also has a small effect on the lateral dimensions of the chains, with a modest increase in the lateral radius of gyration (R_{xy}) for attractive substrates and a slight decrease for repulsive substrates. At $l_B = 3\sigma$ we find $R_{xy} = (6.46 \pm 0.002)\sigma$, $R_{xy} = (6.28 \pm 0.002)\sigma$, and $R_{xy} = (6.21 \pm 0.002)\sigma$ for $\Delta = -1$, $\Delta = 0$, and $\Delta = 1$, respectively.

3.2. Effect of Polymer Charge. We now proceed to vary the Manning parameter ξ by tuning the polymer charge per length and explore how the impacts on brush and ion configuration differ from those observed upon variation of the Bjerrum length. In experimental realizations polymer charge can be controlled, e.g., by pH-induced changes in protonation. To alter it in simulations, we vary the "monomer" charge ranging from $-0.1e$ to $-e$. The results are summarized in Figure 3a. Unlike the expansion−contraction behavior

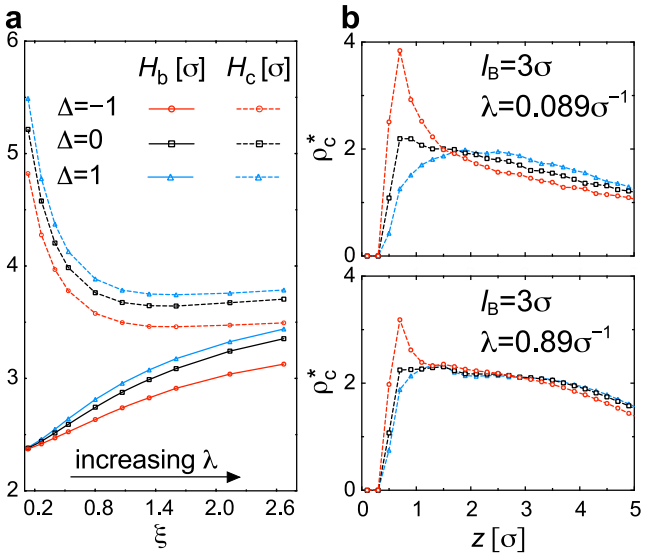

Figure 3. Dependence of brush height, counterion location, and dielectric effects on polymer charge density: (a) Brush height H_b (solid lines) and counterion height H_c (dashed lines) as a function of Manning parameter ξ (tuned by varying the monomer charge). (b) Distributions (normalized by the overall counterion density) of counterions, ρ_c^*, as a function of the distance z to the substrate at Bjerrum length $l_B = 3\sigma$ and polymer charge per length $-e\lambda = -0.089e/\sigma$ (top, monomer charge $-0.1e$) and $-e\lambda = -0.89e/\sigma$ (bottom, monomer charge $-e$).

observed in Figure 2a, a *monotonic* expansion of the brush is found as the coupling ξ is enhanced by increasing λ. This monotonic expansion is in agreement with prior simulations[20,26,31] and can be understood from the persistent dominance of intra- and interpolymer repulsions, which scale as λ^2, over monomer−ion attractions, which tend to reduce the counterion osmotic pressure and thereby counteract the swelling of the brush, but only scale as λ. We note that we still observe absorption of ions into the brush even though the monotonic brush expansion (reflecting an increase in effective polymer charge) contradicts the Manning prediction that the effective polymer charge remains constant above the counterion condensation threshold.

The observed expansion upon increase of λ bears qualitative resemblance to the scaling prediction,[37] although it should be noted that no quantitative agreement is to be expected given the short chain length employed here. In the absence of salt, scaling theory has predicted six different scaling regimes as a function of grafting density and polymer line charge density. When the polymers are weakly charged, the counterion distribution extends beyond the brush and the PEB resides in the Pincus regime, where H_b is predicted to scale as $N^3\Gamma\lambda^2$. In the opposite limit, the counterions are strongly adsorbed within the brush. In this osmotic regime the brush height scales as $N\lambda^{1/2}$. In our system, as we vary the bead charge from $-0.1e$ to $-e$, the PEB initially exhibits behavior similar to the Pincus regime[37] characterized by a rapid expansion, followed by a slowdown in the expansion rate at higher λ, consistent with the osmotic regime.

Dielectric effects on brush structure (i.e., H_b) diminish at low λ as the coupling of the polymers to the polarization charges weakens. Interestingly, the dielectric modulation of counterion location H_c is almost independent of λ. Reflected in the normalized counterion distributions for the PEB with low ($-0.1e$, Figure 3b, top) and high ($-e$) bead charge (Figure 3b, bottom), the persistent dielectric modulation of H_c originates from the interactions of the counterions with their own polarization charges. While both ion distributions show dielectric effects near the interface, at low λ they are particularly prominent. Therein there is almost no polarization charge or electrostatic screening because of the polymers, and the dielectric modulation of ion distribution is unaffected by polymer location due to the rather weak ion−polymer coupling.

3.3. Role of Counterion Valency. Multivalent counterions have the potential to significantly alter the conformation of polyelectrolytes (cf. ref 56 and references therein), including PEBs.[32] Enhanced valency introduces stronger interactions between ions, monomers, and polarization charges and thus potentially also alters the magnitude of dielectric effects. To examine this, we revisit the systems of section 3.1 (variation of solvent permittivity) and section 3.2 (variation of polymer charge), but now using trivalent counterions. We quantify the brush response in Figure 4.

Variation of the Manning parameter by decreasing temperature or solvent permittivity still leads to a nonmonotonic behavior of brush height (Figure 4a). The maximum shifts from $\xi^* \approx 1$ for monovalent counterions (Figure 2a) to $\xi^* \approx 1/3$, qualitatively in line with the onset of trivalent counterion condensation predicted by Manning theory. The collapse at strong coupling is much stronger than for monovalent ions, enhanced by the ability of multivalent ions to cause polyelectrolyte condensation: trivalent ions act as intra- and interpolymer "linkers",[35,56,64] thus enabling a denser packing (Figure 4b). This is also reflected in the simulations by the fraction of trivalent ions binding to more than one chain, which is 16.9% for $l_b = 3\sigma$ and $\Delta = 0$, compared to 2.0% for monovalent counterions.

The dielectric modulation is qualitatively similar to what we observed for monovalent ions, albeit amplified by the quadratically enhanced coupling (cf. eq 4) between multivalent ions and their own polarization charges. The modulation of ion distributions propagates to the polymer brush structure due to the strong coupling between multivalent ions and polymers. The effect of a conducting substrate ($\Delta = -1$) is particularly strong, as trivalent ions can pull the polymer chains to the surface by simultaneously binding to the chains and to the interface (Figure 4b).

https://dx.doi.org/10.1021/acs.macromol.9b02749
Macromolecules 2020, 53, 2983−2990

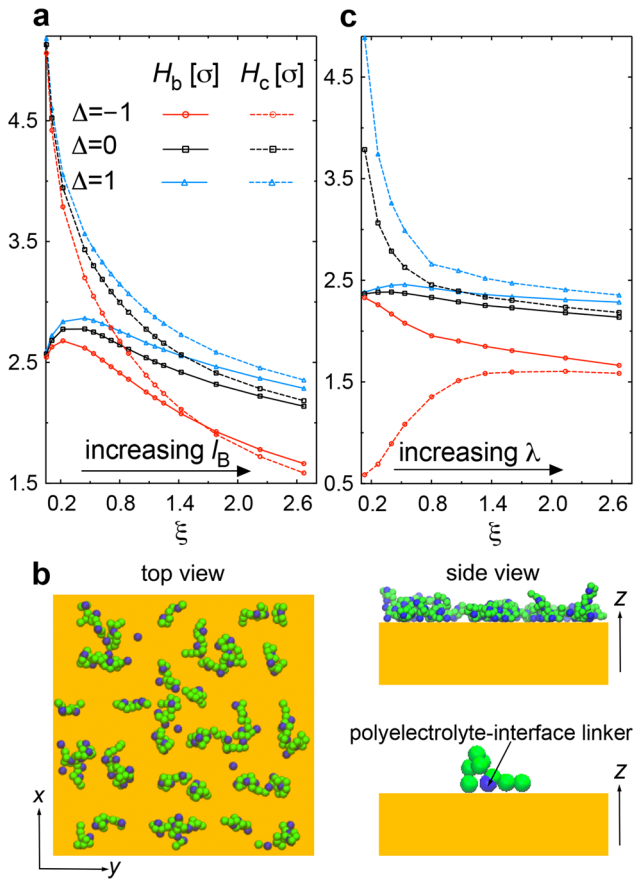

Figure 4. Effect of trivalent counterions on a PEB under salt-free conditions. (a) Brush height H_b (solid lines) and counterion height H_c (dashed lines) as a function of Manning parameter ξ, which is varied by tuning l_b (changing temperature T or solvent permittivity κ_{sol}). (b) A simulation snapshot illustrates that for a brush (green monomers) grafted on a conducting substrate the trivalent counterions (blue) cause, at sufficiently strong coupling ($l_B = 3\sigma$, $\xi \approx 2.67$), both intra- and interpolymer condensation (top view) and simultaneously bind to the polyelectrolyte and to the interface (side view). (c) Same as (a), but now the Manning parameter is varied by tuning the polymer charge density. Comparison to Figure 3a shows that trivalent and monovalent counterions lead to qualitatively different behavior.

We observe considerably more complex behavior upon varying the polymer charge density (Figure 4c). In the absence of surface polarization, we observe nearly constant brush height, with a weak chain contraction for $\xi \gtrsim 1/3$, qualitatively different from the monotonic expansion detected in the presence of monovalent counterions (Figure 3a). The trivalent ions within the brush can counteract the increasing polymer−polymer repulsion as λ is increased, and the PEBs exhibit behavior akin to the collapsed brush regime,[65] where the brush height is predicted to decrease with increasing charge on the polyelectrolyte chains. Dielectric effects further alter this behavior. Whereas a repulsive substrate causes an even weaker collapse with slightly shifted ξ^* and expanded brush structure compared to a nonpolarizable substrate, the brush on a conducting interface shows a markedly different trend, namely, a strong monotonic contraction. This observation underlines that surface polarization can *qualitatively* alter the response of a PEB to variation of conditions such as pH.

Interestingly, the average counterion location H_c for a brush grafted on a conducting substrate *increases* monotonically, contrasting strongly with the behavior observed for monovalent counterions (Figure 3a) and for trivalent counterions near insulating or nonpolarizable substrates (Figure 4c). At low polymer charge density, the strong interaction of trivalent ions with their induced polarization charges dictates the ion distribution and leads to ion accumulation near the substrate (conversely, it is responsible for their exclusion near a low-permittivity substrate). However, at high λ, strong ion−polymer binding competes with the ion−polarization charge interactions. As a result, the ions detach from the interface and H_c increases. The strong binding of ions to the substrate also explains the observed monotonic contraction of the brush for $\Delta = -1$. Instead of adsorption of ions from the bulk into the brush, upon increase of λ the polymers are attracted to the layer of counterions already residing near the interface.

3.4. Effect of Counterion Size. In all simulations presented above, we employed counterions with the same size as the monomers, $\sigma_c = \sigma_b$. However, ion size affects counterion binding, as it determines the closest distance between ions and monomers,[66] so that smaller size results in a stronger interaction—an effect analogous to increasing the ion valency. We therefore anticipate that counterion size can modify the brush height as well as the magnitude of dielectric effects and once more revisit the systems studied in sections 3.1 and 3.2, for both smaller ($\sigma_c = 0.5\sigma_b$) and larger monovalent counterions ($\sigma_c = 2\sigma_b$). A comparison for the three counterion sizes is presented in Figure 5.

Smaller ion size results in a more compact brush structure, in agreement with simulations of free polyelectrolytes.[67] The enhanced ion−polymer binding also causes an earlier onset of counterion condensation and stronger intra- and interpolymer screening, as manifested by the shift in ξ^* to smaller values when ξ is varied via the Bjerrum length (Figure 5a) and by a slower expansion when ξ is varied via the polymer charge density (Figure 5b). In fact, for the larger ion size ($\sigma_c = 2\sigma_b$) studied, the brush height becomes a monotonic function of ξ in Figure 5a, and ξ^* is no longer detected within the range studied, reflecting that the larger ion size suppresses the condensation of counterions onto the chains (for bead charge $-e$ and $l_B = 3\sigma$, only 13.7% of ions are bound when $\sigma_c = 2\sigma_b$, compared to 73.5% for $\sigma_c = \sigma_b$) and also swells the brush due to enhanced excluded volume of those ions that remain in the brush.

Smaller counterions also enhance the dielectric effects on brush structure. The enhancement is weak for low-permittivity substrates, but for brushes grafted onto conducting substrates decreasing the ion size has a stronger effect since, in addition to enhancing the ion−polymer coupling, it allows the ions to approach the interface more closely and thereby couple more strongly to surface polarization charges.

3.5. Effect of Ion Concentration. Dielectric effects are expected to be increasingly screened out as the ion concentration in the system increases. To confirm this, we consider two independent ways of changing this concentration, namely tuning either the salt concentration c (Figure 6a) or the polymer grafting density Γ (Figure 6b).

For monovalent salt, scaling theory[37] predicts a "salted brush regime" where the salt concentration c is high enough to modify the brush structure, decreasing the brush height H_b as $c^{-1/3}$. This contraction is due to a reduction in the counterion osmotic pressure and the electrostatic repulsion between

https://dx.doi.org/10.1021/acs.macromol.9b02749
Macromolecules 2020, 53, 2983−2990

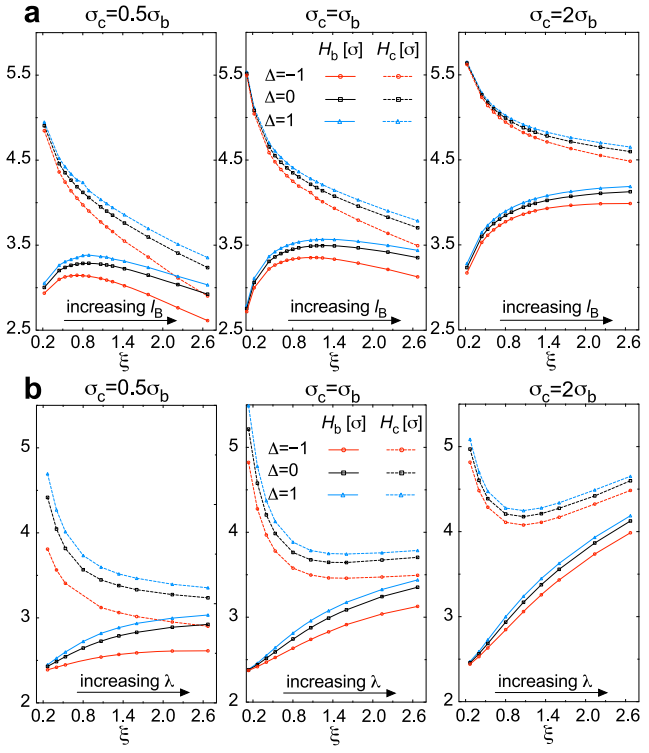

Figure 5. Role of ion size. Brush height H_b (solid lines) and counterion height H_c (dashed lines) as a function of Manning parameter ξ which is adjusted by changing either (a) the Bjerrum length l_B or (b) the polymer charge density. The salt-free PEB is neutralized by monovalent counterions of size $\sigma_c = 0.5\sigma_b$ (panels in the left column), $\sigma_c = \sigma_b$ (panels in the central column), and $\sigma_c = 2\sigma_b$ (panels in the right column).

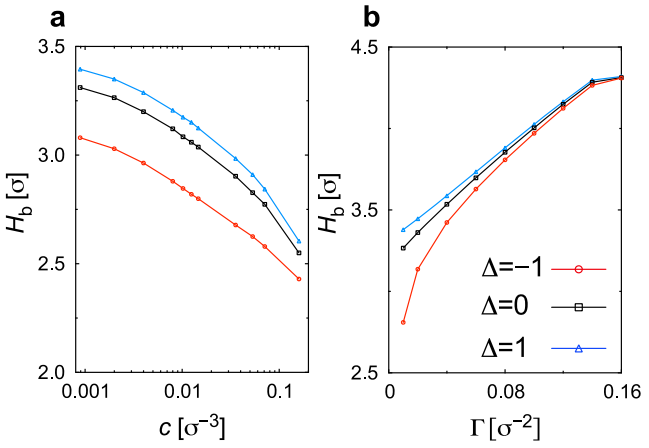

Figure 6. Effect of ion concentration on the brush structure and magnitude of dielectric effects. Brush height H_b as a function of (a) monovalent salt concentration c and (b) polymer grafting density Γ at fixed Manning parameter $\xi \approx 2.67$ with conducting ($\Delta = -1$), insulating ($\Delta = 1$), and nonpolarizable ($\Delta = 0$) substrates.

polymers.[36,37] Even though our chains are too short to be described by the scaling prediction, Figure 6a qualitatively confirms this behavior. Along with this, the role of dielectric mismatch diminishes with increasing salt concentration, as expected.

The opposite trend in H_b occurs when the grafting density is increased (Figure 6b). We ascribe the observed swelling of the brush to the enhancement of interpolymer electrostatic repulsion, steric repulsion, and counterion osmotic pressure. The latter increases despite the strong counterion condensation because of the reduction in free volume available to the ions. Interestingly, early scaling theories[36,37] predict a brush height in this "osmotic regime" independent of grafting density. One assumption underlying these derivations is that the chain free energy is described by the "weak-stretching" regime. In our simulations, even for the lowest grafting density ($\Gamma = 0.02\sigma^{-2}$) the chains are stretched up to ~65% of their contour length ($\approx 2^{1/6}\sigma N$) and hence more likely described by the strongly stretched regime (i.e., nonlinear elasticity).[30] However, this does not resolve the discrepancy; rather, inclusion in the counterion entropy of the finite volume of the polymer is what gives rise to a brush height that grows linearly with grafting density. This matches our simulation results, which in turn reproduce earlier simulation work.[68]

Although the response to an increase in grafting density is markedly different from the response to an increase in salt concentration, Figure 6b confirms that dielectric modulation of the brush height again diminishes at higher ion concentration.

3.6. Effect of Electric Field. Lastly, we consider the deformation of a PEB under an external electric field oriented parallel to the substrate. Such a field offers an approach for regulating solvent transport in a nanochannel,[5,6] where the magnitude of the electric field affects whether the channel is open or closed. Exploration of the role of dielectric mismatch on transport in PEB-functionalized nanochannels was one of the motivations for our earlier work.[54] Here we examine the corresponding deformation of the brush at two selected grafting densities, $\Gamma = 0.02\sigma^{-2}$ and $\Gamma = 0.04\sigma^{-2}$.

Figure 7 illustrates that for both grafting densities and all substrate permittivities the brush height decreases with

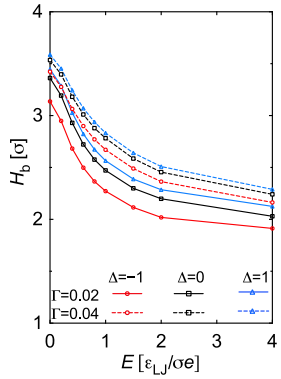

Figure 7. Polymer brush under an external electric field parallel to the substrate. Brush height H_b is shown as a function of field strength E at fixed Manning parameter $\xi \approx 2.67$ for two different grafting densities Γ. Lower grafting densities permit stronger deformation of the brush and conducting substrates yield the most compact brush.

increasing electric field, opening the channel by pressing the chains toward the substrate. As expected, PEBs at lower grafting density respond more strongly to an applied field since the polymers have more configurational freedom to deform. The effect of dielectric mismatch on brush structure is present at all field strengths, with conducting substrates systematically yielding a more compact brush and therefore a larger effective width of the nanochannel.

https://dx.doi.org/10.1021/acs.macromol.9b02749
Macromolecules 2020, 53, 2983−2990

4. CONCLUSIONS

Employing coarse-grained molecular dynamics simulations, we have examined how the response of polyelectrolyte brushes to changes in various intrinsic and external conditions depends on the dielectric properties of the substrate. Compared to substrates that have no dielectric mismatch with the solvent, polyelectrolyte brushes on conducting interfaces adopt contracted configurations, whereas brushes on low-permittivity interfaces are expanded. The effect of the latter is relatively weaker because of the constraint introduced by the polyelectrolyte−substrate grafting. The dielectric modulation of brush structure is amplified at high Bjerrum length, low salt concentration, low grafting density, small counterion size, high polymer charge, and high counterion valency.

In the particular case of multivalent counterions, surface polarization can qualitatively alter the response of a polyelectrolyte brush to varying polymer charge density, e.g., due to a change in pH. Notably, in such systems, the multivalent ions can cause a collapse of the brush onto a conducting substrate when the polymer charge is increased, whereas the brush is relatively insensitive to polymer charge when grafted onto an insulating substrate.

Even though the work presented here employs model systems with a low degree of polymerization, we foresee our findings to be of relevance in nanoscale applications where precise control over brush structure and ion behavior are needed.

AUTHOR INFORMATION

Corresponding Author

Erik Luijten − *Department of Materials Science and Engineering, Department of Engineering Sciences and Applied Mathematics, Department of Chemistry, and Department of Physics and Astronomy, Northwestern University, Evanston, Illinois 60208, United States;* orcid.org/0000-0003-2364-1866; Email: luijten@northwestern.edu

Authors

Jiaxing Yuan − *School of Physics and Astronomy and Institute of Natural Sciences, Shanghai Jiao Tong University, Shanghai 200240, China;* orcid.org/0000-0001-9890-4961

Hanne S. Antila − *Department of Materials Science and Engineering, Northwestern University, Evanston, Illinois 60208, United States; Department of Theory and Bio-Systems, Max Planck Institute of Colloids and Interfaces, 14476 Potsdam, Germany;* orcid.org/0000-0002-2474-5053

Complete contact information is available at: https://pubs.acs.org/10.1021/acs.macromol.9b02749

Author Contributions

J.Y. and H.S.A. contributed equally to this work.

Notes

The authors declare no competing financial interest.

ACKNOWLEDGMENTS

This material is based upon work supported by the U.S. National Science Foundation under Grant DMR-1610796.

REFERENCES

(1) Das, S.; Banik, M.; Chen, G.; Sinha, S.; Mukherjee, R. Polyelectrolyte brushes: theory, modelling, synthesis and applications. *Soft Matter* **2015**, *11*, 8550−8583.

(2) Tagliazucchi, M.; Szleifer, I. Transport mechanisms in nanopores and nanochannels: can we mimic nature? *Mater. Today* **2015**, *18*, 131−142.

(3) Yameen, B.; Ali, M.; Neumann, R.; Ensinger, W.; Knoll, W.; Azzaroni, O. Ionic transport through single solid-state nanopores controlled with thermally nanoactuated macromolecular gates. *Small* **2009**, *5*, 1287−1291.

(4) Guo, W.; Xia, H.; Xia, F.; Hou, X.; Cao, L.; Wang, L.; Xue, J.; Zhang, G.; Song, Y.; Zhu, D.; Wang, Y.; Jiang, L. Current rectification in temperature-responsive single nanopores. *ChemPhysChem* **2010**, *11*, 859−864.

(5) Ouyang, H.; Xia, Z.; Zhe, J. Voltage-controlled flow regulating in nanofluidic channels with charged polymer brushes. *Microfluid. Nanofluid.* **2010**, *9*, 915−922.

(6) Cao, Q.; Zuo, C.; Li, L.; Zhang, Y.; Yan, G. Electro-osmotic flow in nanochannels with voltage-controlled polyelectrolyte brushes: Dependence on grafting density and normal electric field. *J. Polym. Sci., Part B: Polym. Phys.* **2012**, *50*, 805−811.

(7) Weir, M. P.; Heriot, S. Y.; Martin, S. J.; Parnell, A. J.; Holt, S. A.; Webster, J. R. P.; Jones, R. A. L. Voltage-induced swelling and deswelling of weak polybase brushes. *Langmuir* **2011**, *27*, 11000−11007.

(8) Ito, Y.; Inaba, M.; Chung, D.-J.; Imanishi, Y. Control of water permeation by pH and ionic strength through a porous membrane having poly(carboxylic acid) surface-grafted. *Macromolecules* **1992**, *25*, 7313−7316.

(9) Ito, Y.; Park, Y. S.; Imanishi, Y. Nanometer-sized channel gating by a self-assembled polypeptide brush. *Langmuir* **2000**, *16*, 5376−5381.

(10) Park, Y. S.; Ito, Y.; Imanishi, Y. Photocontrolled gating by polymer brushes grafted on porous glass filter. *Macromolecules* **1998**, *31*, 2606−2610.

(11) Azzaroni, O.; Moya, S.; Farhan, T.; Brown, A. A.; Huck, W. T. S. Switching the properties of polyelectrolyte brushes via "hydrophobic collapse. *Macromolecules* **2005**, *38*, 10192−10199.

(12) Zhou, F.; Huck, W. T. S. Three-stage switching of surface wetting using phosphate-bearing polymer brushes. *Chem. Commun.* **2005**, 5999−6001.

(13) Berger, S.; Synytska, A.; Ionov, L.; Eichhorn, K.-J.; Stamm, M. Stimuli-responsive bicomponent polymer Janus particles by "grafting from"/"grafting to" approaches. *Macromolecules* **2008**, *41*, 9669−9676.

(14) Hariharan, R.; Biver, C.; Mays, J.; Russel, W. B. Ionic strength and curvature effects in flat and highly curved polyelectrolyte brushes. *Macromolecules* **1998**, *31*, 7506−7513.

(15) Kumar, N. A.; Seidel, C. Polyelectrolyte brushes with added salt. *Macromolecules* **2005**, *38*, 9341−9350.

(16) Wynveen, A.; Likos, C. N. Interactions between planar polyelectrolyte brushes: effects of stiffness and salt. *Soft Matter* **2010**, *6*, 163−171.

(17) He, S.-z.; Merlitz, H.; Chen, L.; Sommer, J.-U.; Wu, C.-X. Polyelectrolyte brushes: MD simulation and SCF theory. *Macromolecules* **2010**, *43*, 7845−7851.

(18) Goujon, F.; Ghoufi, A.; Malfreyt, P.; Tildesley, D. J. Frictional forces in polyelectrolyte brushes: effects of sliding velocity, solvent quality and salt. *Soft Matter* **2012**, *8*, 4635−4644.

(19) Guptha, V. S.; Hsiao, P. Y. Polyelectrolyte brushes in monovalent and multivalent salt solutions. *Polymer* **2014**, *55*, 2900−2912.

(20) Kinjo, T.; Yoshida, H.; Washizu, H. Coarse-grained simulations of polyelectrolyte brushes using a hybrid model. *Colloid Polym. Sci.* **2018**, *296*, 441−449.

(21) Sandberg, D. J.; Carrillo, J.-M. Y.; Dobrynin, A. V. Molecular dynamics simulations of polyelectrolyte brushes: From single chains to bundles of chains. *Langmuir* **2007**, *23*, 12716−12728.

(22) Carrillo, J.-M. Y.; Dobrynin, A. V. Morphologies of planar polyelectrolyte brushes in a poor solvent: Molecular dynamics simulations and scaling analysis. *Langmuir* **2009**, *25*, 13158−13168.

(23) He, G.-L.; Merlitz, H.; Sommer, J.-U. Molecular dynamics simulations of polyelectrolyte brushes under poor solvent conditions: Origins of bundle formation. *J. Chem. Phys.* **2014**, *140*, 104911.
(24) Seidel, C. Strongly stretched polyelectrolyte brushes. *Macromolecules* **2003**, *36*, 2536−2543.
(25) Hehmeyer, O. J.; Arya, G.; Panagiotopoulos, A. Z.; Szleifer, I. Monte Carlo simulation and molecular theory of tethered polyelectrolytes. *J. Chem. Phys.* **2007**, *126*, 244902.
(26) Ouyang, H.; Xia, Z.; Zhe, J. Static and dynamic responses of polyelectrolyte brushes under external electric field. *Nanotechnology* **2009**, *20*, 195703.
(27) Cao, Q.; Zuo, C.; Li, L.; Yan, G. Effects of chain stiffness and salt concentration on responses of polyelectrolyte brushes under external electric field. *Biomicrofluidics* **2011**, *5*, 044119.
(28) Ho, Y.-F.; Shendruk, T. N.; Slater, G. W.; Hsiao, P.-Y. Structure of polyelectrolyte brushes subject to normal electric fields. *Langmuir* **2013**, *29*, 2359−2370.
(29) Csajka, F. S.; Netz, R. R.; Seidel, C.; Joanny, J.-F. Collapse of polyelectrolyte brushes: Scaling theory and simulations. *Eur. Phys. J. E: Soft Matter Biol. Phys.* **2001**, *4*, 505−513.
(30) Naji, A.; Netz, R. R.; Seidel, C. Non-linear osmotic brush regime: Simulations and mean-field theory. *Eur. Phys. J. E: Soft Matter Biol. Phys.* **2003**, *12*, 223−237.
(31) Li, L.; Cao, Q.; Zuo, C. Effect of counterion valence on conformational behavior of spherical polyelectrolyte brushes confined between two parallel walls. *Polymers* **2018**, *10*, 363.
(32) Mei, Y.; Lauterbach, K.; Hoffmann, M.; Borisov, O. V.; Ballauff, M.; Jusufi, A. Collapse of spherical polyelectrolyte brushes in the presence of multivalent counterions. *Phys. Rev. Lett.* **2006**, *97*, 158301.
(33) Jackson, N. E.; Brettmann, B. K.; Vishwanath, V.; Tirrell, M.; de Pablo, J. J. Comparing solvophobic and multivalent induced collapse in polyelectrolyte brushes. *ACS Macro Lett.* **2017**, *6*, 155−160.
(34) Liu, L.; Pincus, P. A.; Hyeon, C. Heterogeneous morphology and dynamics of polyelectrolyte brush condensates in trivalent counterion solution. *Macromolecules* **2017**, *50*, 1579−1588.
(35) Yu, J.; Jackson, N. E.; Xu, X.; Brettmann, B. K.; Ruths, M.; de Pablo, J. J.; Tirrell, M. Multivalent ions induce lateral structural inhomogeneities in polyelectrolyte brushes. *Sci. Adv.* **2017**, *3*, No. eaao1497.
(36) Pincus, P. Colloid stabilization with grafted polyelectrolytes. *Macromolecules* **1991**, *24*, 2912−2919.
(37) Borisov, O. V.; Zhulina, E. B.; Birshtein, T. M. Diagram of the states of a grafted polyelectrolyte layer. *Macromolecules* **1994**, *27*, 4795−4803.
(38) Desai, P. R.; Sinha, S.; Das, S. Polyelectrolyte brush bilayers in weak interpenetration regime: Scaling theory and molecular dynamics simulations. *Phys. Rev. E: Stat. Phys., Plasmas, Fluids, Relat. Interdiscip. Top.* **2018**, *97*, 032503.
(39) Chen, H.; Zajac, R.; Chakrabarti, A. Conformational properties of polyelectrolyte brushes: A Monte Carlo and self-consistent-field study. *J. Chem. Phys.* **1996**, *104*, 1579−1588.
(40) Zhulina, E. B.; Borisov, O. V. Structure and interaction of weakly charged polyelectrolyte brushes: Self-consistent field theory. *J. Chem. Phys.* **1997**, *107*, 5952−5967.
(41) Zhulina, E. B.; Klein Wolterink, J.; Borisov, O. V. Screening effects in a polyelectrolyte brush: A Self-consistent-field theory. *Macromolecules* **2000**, *33*, 4945−4953.
(42) Chen, L.; Merlitz, H.; He, S.-z.; Wu, C.-X.; Sommer, J.-U. Polyelectrolyte brushes: Debye approximation and mean-field theory. *Macromolecules* **2011**, *44*, 3109−3116.
(43) Lebedeva, I. O.; Zhulina, E. B.; Borisov, O. V. Self-consistent field theory of polyelectrolyte brushes with finite chain extensibility. *J. Chem. Phys.* **2017**, *146*, 214901.
(44) Jiang, T.; Li, Z.; Wu, J. Structure and swelling of grafted polyelectrolytes: Predictions from a nonlocal density functional theory. *Macromolecules* **2007**, *40*, 334−343.
(45) Guo, X.; Ballauff, M. Spatial dimensions of colloidal polyelectrolyte brushes as determined by dynamic light scattering. *Langmuir* **2000**, *16*, 8719−8726.
(46) Guo, X.; Zhao, K. Dielectric analysis based on spherical-shell model for cationic and anionic spherical polyelectrolyte brushes. *J. Phys.: Condens. Matter* **2017**, *29*, 295101.
(47) Merlitz, H.; Li, C.; Wu, C.; Sommer, J.-U. Polyelectrolyte brushes in external fields: molecular dynamics simulations and mean-field theory. *Soft Matter* **2015**, *11*, 5688−5696.
(48) Tergolina, V. B.; dos Santos, A. P. Effect of dielectric discontinuity on a spherical polyelectrolyte brush. *J. Chem. Phys.* **2017**, *147*, 114103.
(49) Motornov, M.; Tam, T. K.; Pita, M.; Tokarev, I.; Katz, E.; Minko, S. Switchable selectivity for gating ion transport with mixed polyelectrolyte brushes: Approaching 'smart' drug delivery systems. *Nanotechnology* **2009**, *20*, 434006.
(50) Yameen, B.; Ali, M.; Neumann, R.; Ensinger, W.; Knoll, W.; Azzaroni, O. Synthetic proton-gated ion channels via single solid-state nanochannels modified with responsive polymer brushes. *Nano Lett.* **2009**, *9*, 2788−2793.
(51) Yameen, B.; Ali, M.; Neumann, R.; Ensinger, W.; Knoll, W.; Azzaroni, O. Single conical nanopores displaying pH-tunable rectifying characteristics. Manipulating ionic transport with zwitterionic polymer brushes. *J. Am. Chem. Soc.* **2009**, *131*, 2070−2071.
(52) Silies, L.; Andrieu-Brunsen, A. Programming ionic pore accessibility in zwitterionic polymer modified nanopores. *Langmuir* **2018**, *34*, 807−816.
(53) Park, S.-J.; Taton, T. A.; Mirkin, C. A. Array-based electrical detection of DNA with nanoparticle probes. *Science* **2002**, *295*, 1503−1506.
(54) Yuan, J.; Antila, H. S.; Luijten, E. Dielectric effects on ion transport in polyelectrolyte brushes. *ACS Macro Lett.* **2019**, *8*, 183−187.
(55) Stevens, M. J.; Kremer, K. Structure of salt-free linear polyelectrolytes. *Phys. Rev. Lett.* **1993**, *71*, 2228−2231.
(56) Hsiao, P.-Y.; Luijten, E. Salt-induced collapse and reexpansion of highly charged flexible polyelectrolytes. *Phys. Rev. Lett.* **2006**, *97*, 148301.
(57) Hockney, R. W.; Eastwood, J. W. *Computer Simulation Using Particles*; McGraw-Hill: New York, 1981.
(58) Thomson, W. Geometrical investigations with reference to the distribution of electricity on spherical conductors. *Camb. Dublin Math. J.* **1848**, *3*, 141−148.
(59) Jackson, J. D. *Classical Electrodynamics*, 3rd ed.; Wiley: New York, 1999.
(60) Yeh, I.-C.; Berkowitz, M. L. Ewald summation for systems with slab geometry. *J. Chem. Phys.* **1999**, *111*, 3155−3162.
(61) Manning, G. S. Limiting laws and counterion condensation in polyelectrolyte solutions I. Colligative properties. *J. Chem. Phys.* **1969**, *51*, 924−933.
(62) Winkler, R. G.; Gold, M.; Reineker, P. Collapse of polyelectrolyte macromolecules by counterion condensation and ion pair formation: A molecular dynamics simulation study. *Phys. Rev. Lett.* **1998**, *80*, 3731−3735.
(63) Messina, R. Effect of image forces on polyelectrolyte adsorption at a charged surface. *Phys. Rev. E* **2004**, *70*, 051802. Erratum: *Phys. Rev. E* **2006**, *74*, 049906.
(64) Solis, F. J.; Olvera de la Cruz, M. Collapse of flexible polyelectrolytes in multivalent salt solutions. *J. Chem. Phys.* **2000**, *112*, 2030−2035.
(65) Santangelo, C. D.; Lau, A. W. C. Effects of counterion fluctuations in a polyelectrolyte brush. *Eur. Phys. J. E: Soft Matter Biol. Phys.* **2004**, *13*, 335−344.
(66) Pack, G. R.; Lamm, G. Counterion condensation theory revisited: Limits on its applicability. *Int. J. Quantum Chem.* **1993**, *48*, 213−230.
(67) Gordievskaya, Y. D.; Kramarenko, E. Y. Effect of counterion size on the structure of a flexible polyelectrolyte chain in low-polar solvents. *Polym. Sci., Ser. C* **2018**, *60*, 37−48.
(68) Csajka, F. S.; Seidel, C. Strongly charged polyelectrolyte brushes: A molecular dynamics study. *Macromolecules* **2000**, *33*, 2728−2739.

https://dx.doi.org/10.1021/acs.macromol.9b02749
Macromolecules 2020, 53, 2983−2990